Electronic Supplementary Information

Carbon nanobowls supported chemical functionalized PtRh nanocrystals: A highly active and methanol tolerant electrocatalyst towards oxygen reduction reaction

Ze-Nong Zhang,[a] Bo-Qiang Miao,[b] Zhu-Qing Wu,[a] Pei Chen,[b] Xue Xiao,*[c] Shu-Ni Li,*[a] and Yu Chen[b]

[a] Key Laboratory of Macromolecular Science of Shaanxi Province, School of Chemistry and Chemical Engineering, Shaanxi Normal University, Xi'an 710062, PR China.

[b] School of Materials Science and Engineering, Shaanxi Normal University, Xi'an 710062, PR China.

[c] Centre for Translational Atomaterials, School of Science, Computing and Engineering Technologies, Swinburne University of Technology, Hawthorn, VIC 3122, Australia.

* Corresponding authors

E-mails: lishuni@snnu.edu.cn (S. Li); tiffanyxx110@gmail.com (X. Xiao)

The preparation of working electrode

The electrocatalyst covered glassy carbon working electrode was prepared according to the previously reported procedure.[1, 2] Briefly, the electrocatalyst suspension was achieved by ultrasonic mixing 8 mg of electrocatalyst and 4 mL of isopropanol/Nafion® solution (20% isopropanol and 0.02% Nafion®) for 1 h. Then, 10 μL of electrocatalyst ink was drop-coated on a clean glassy carbon electrode and dried at room temperature. Finally, the working electrode was put in an electrochemical cell containing 0.5 M H_2SO_4 electrolyte for electrochemical measurement.

Measurement of ECSA

The ECSA value of electrocatalyst was achieved from equation 1 by integrating H desorption charge.

$$ECSA = \frac{Q}{m \times C} \quad (1)$$

where Q was the charge in the H desorption region at CV curve, m was the noble metal loading amount on the working electrode, and C (210 μC cm^{-2}) was monolayer hydrogen adsorption charge on noble metal surface. [1, 2].

Calculation of ORR kinetic parameters

Based on the ORR polarization curves, the kinetic current density (i_k) of ORR at electrocatalyst was calculated using Koutecky-Levich equation (eq. 2).

$$\begin{aligned} \frac{1}{i} &= \frac{1}{i_k} + \frac{1}{id} \\ &= \frac{1}{ik} + \frac{1}{\omega B^{1/2}} \\ &= \frac{1}{i_k} + \frac{1}{0.62nFA_{geo}D^{2/3}B^{1/2}\nu^{-1/6}Co_2} \end{aligned} \quad (2)$$

where i was the measured ORR current density, i_k was the kinetic current density, i_d was the ORR diffusion limited current density, B was a constant (*i.e.*, Levich slope), and ω was the rotation rate, n was electron transfer number, F was the Faraday constant, A_{geo} was the geometric surface area of working electrode, D was the diffusion coefficient of O_2 molecule, ν was the kinematic viscosity of electrolyte, and C_{O2} was the concentration of O_2 in electrolyte. Meanwhile, the ORR electron transfer number (n) could be determined from Levich slope (B).

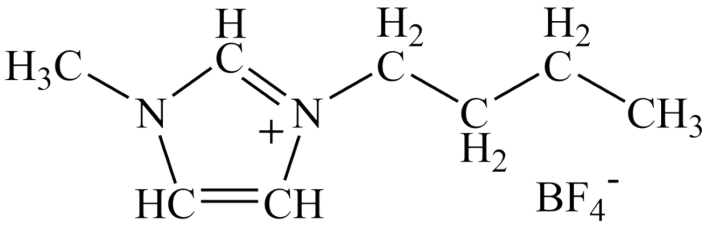

Scheme S1. The structure of $BmimBF_4$.

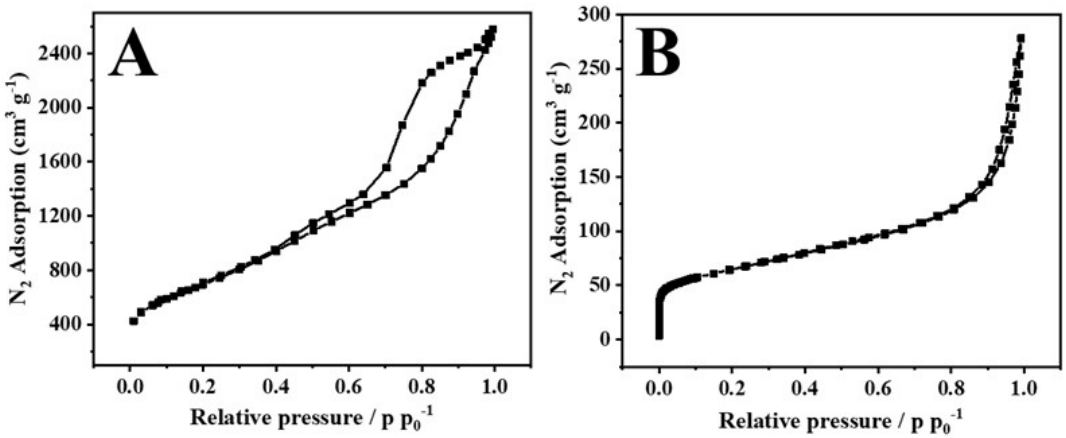

Figure S1. N_2 adsorption–desorption isotherms of (A) carbon nanobowls and (B) Vulcan XC-72.

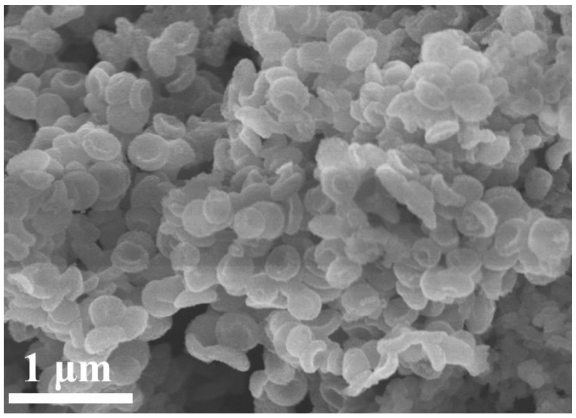

Figure S2. SEM image of Pt_1Rh_1@$BmimBF_4$/CNBs nanohybrids.

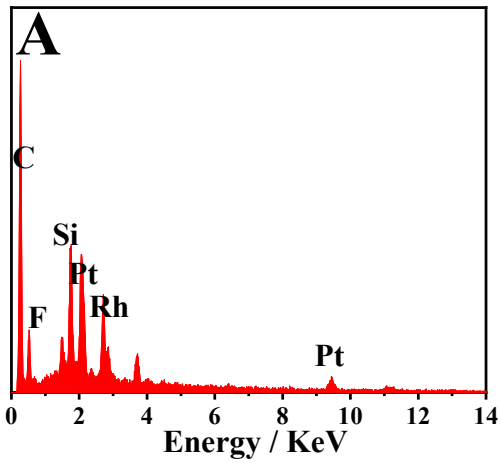

Figure S3. EDX pattern of Pt_1Rh_1@$BmimBF_4$/CNBs nanohybrids. Herein, the strong Si signal comes from Si substrate.

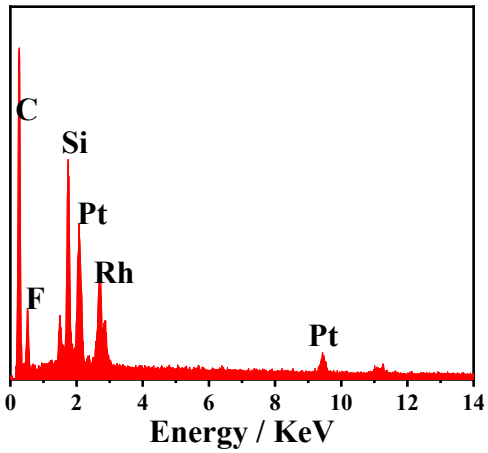

Figure S4. SEM-EDX elemental maps mixed $BmimBF_4$-Pt^{II}+$BmimBF_4$-Rh^{III} complex precipitates.-

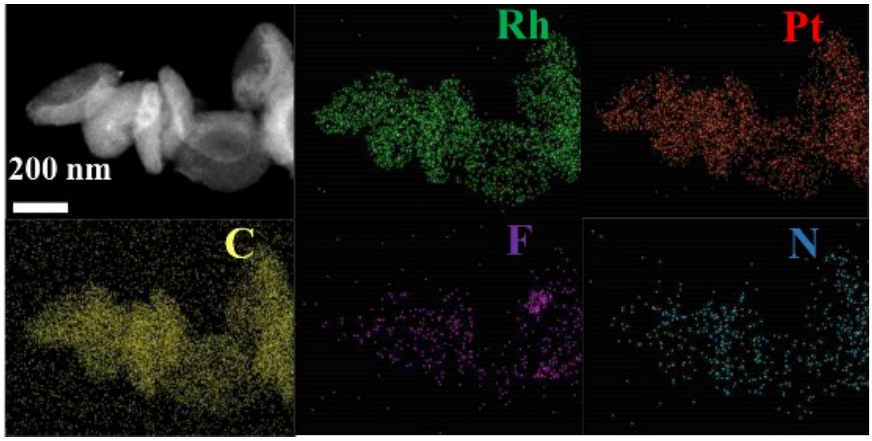

Figure S5. HAADF-STEM and EDX elemental maps of Pt_1Rh_1@$BmimBF_4$/CNBs.

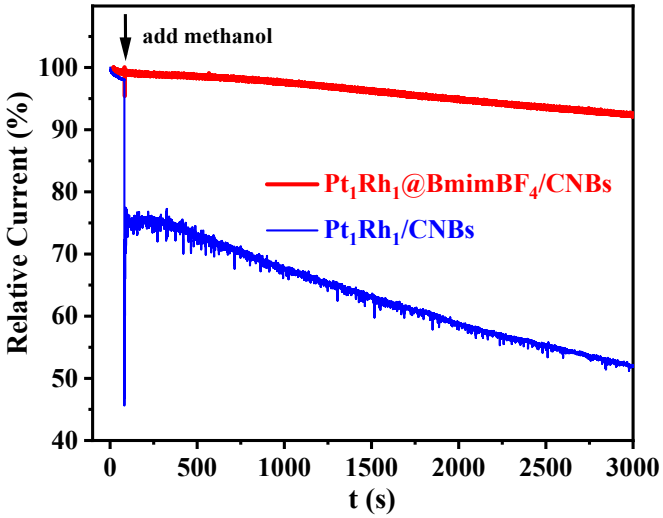

Figure S6. I-t curves of Pt_1Rh_1@$BmimBF_4$/CNBs and Pt_1Rh_1/CNBs.

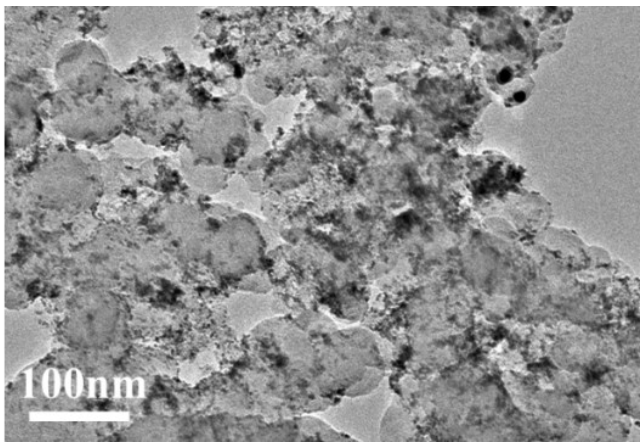

Figure S7. TEM image of commercial Pt/C electrocatalyst.

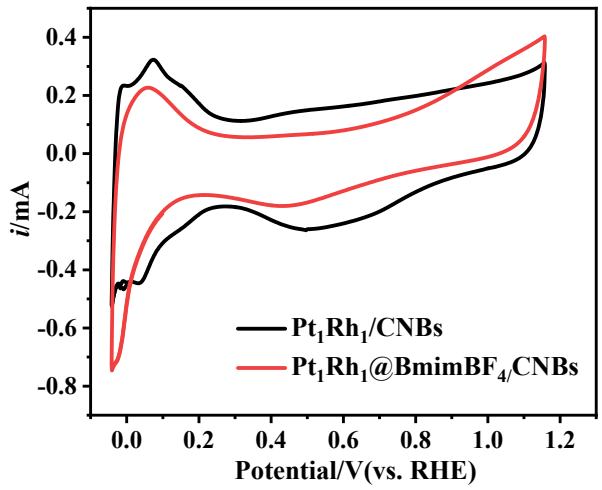

Figure S8. CV curves of Pt_1Rh_1@$BmimBF_4$/CNBs and Pt_1Rh_1/CNBs without

$BmimBF_4$ in N_2-saturated 0.5 M H_2SO_4 solutions at 50 mV s^{-1}. Pt_1Rh_1 /CNBs without $BmimBF_4$ were obtained by the following procedure. At first, 2 mL of 0.05 M mercaptoacetic acid solution was added into 10 mL of 1 mg mL^{-1} Pt_1Rh_1@$BmimBF_4$/CNBs suspension, and stirred for 24 h. In this process, $BmimBF_4$ molecules bound on PtRh surface were replaced by mercaptoacetic acid due to strong S-metal bond interaction. Then, the mercaptoacetic acid modified Pt_1Rh_1/CNBs were treated with UV/ozone (wavelength at 185 and 254 nm in air for 4 h) to remove mercaptoacetic acid. After removal of $BmimBF_4$, ECSA of Pt_1Rh_1/CNBs is estimated to be 77.91 m^2 g^{-1}, showing the surface coverage of $BmimBF_4$ layers on Pt_1Rh_1@$BmimBF_4$/CNBs is only 19.4%.

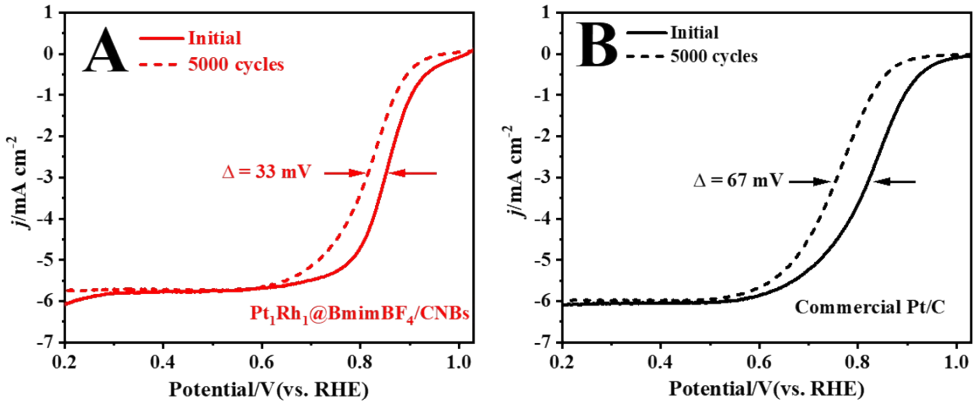

Figure S9. ORR polarization curves of (A) Pt_1Rh_1@$BmimBF_4$/CNBs and (B) Pt/C electrocatalyst before and after accelerated durability tests O_2-purged 0.5 M H_2SO_4 electrolyte at 1600 rpm and at 5 mV s^{-1}.

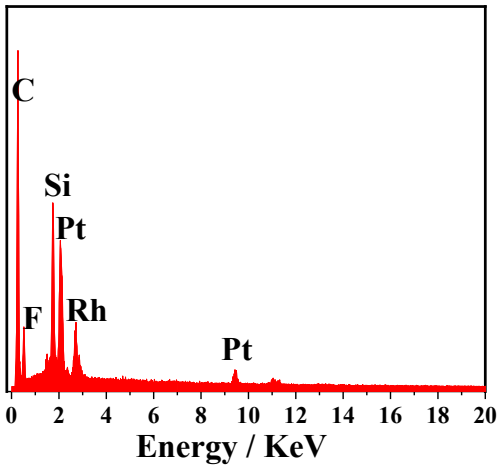

Figure S10. EDX spectrum Pt_1Rh_1@$BmimBF_4$/CNBs after durability test.

Table S1. The $E_{1/2}$ and/or E_{onse} values of ORR at various Pt-based electrocatalysts in H_2SO_4 electrolyte

Electrocatalyst	electrolyte	$E_{1/2}$ (V)	E_{onset} (V)	Ref.
Pt_1Rh_1@$BmimBF_4$/CNBs	0.5 M H_2SO_4	0.85	0.99	This work
Pt/N-doped carbon	0.5 M H_2SO_4	0.88	0.95	2021[3]
Pt-CeOx nanowire/C	0.5 M H_2SO_4	ca. 0.72	0.93	2021[4]
Pt hollow tetrapods	0.5 M H_2SO_4	0.83	1.06	2021[5]
Pt@Ni-N-C nanocomplexes	0.5 M H_2SO_4	0.85	ca. 0.92	2020[6]
Pt/N-doped graphene	0.5 M H_2SO_4	0.868	0.94	2020[7]
Pt nanoparticles/carbon nanotube	0.5 M H_2SO_4	ca. 0.66	0.98	2020[8]
Pt_7Y_3 nanoparticles	0.5 M H_2SO_4	ca. 0.56	ca. 0.80	2020[9]
Pt/Ir/XC72	0.5 M H_2SO_4	ca. 0.76	ca. 0.88	2020[10]
Pt/TiN	0.5 M H_2SO_4	ca. 0.87	ca. 0.96	2020[11]
Pt/rGO+Ir/carbon nanotube	0.5 M H_2SO_4	ca. 0.81	ca. 0.90	2020[12]
PtRuFeCo/rGO	0.5 M H_2SO_4	ca. 0.75	ca. 0.86	2019[13]
Pt_3Sc/carbon nanotubes	0.5 M H_2SO_4	0.68	0.89	2019[14]
Pd_3Y nanoparticles	0.1 M H_2SO_4	0.851	ca.0.98	2019[15]
Pt-WP- graphene nanosheet	0.5 M H_2SO_4	0.61	ca. 0.85	2018[16]

References

1 G.-R. Xu, B. Wang, J.-Y. Zhu, F.-Y. Liu, Y. Chen, J.-H. Zeng, J.-X. Jiang, Z.-H. Liu, Y.-W. Tang and J.-M. Lee, *ACS Catal.*, 2016, **6**, 5260-5267.

2 Q. Xue, J. Bai, C. Han, P. Chen, J.-X. Jiang and Y. Chen, *ACS Catal.*, 2018, **8**, 11287-11295.

3 D. Ganguly, K. Ramanujam and S. Ramaprabhu, *J. Electrochem. Soc.*, 2021, **168**, 064517.

4 S. Chauhan, T. Mori, T. Kobayashi, S. Yamamoto, S. Ito, G. Auchterlonie, R. Wepf, S. Ueda and F. Ye, *J. Am. Ceram. Soc.*, 2021, **104**, 1945-1952.

5 M. Li, A. Yang, S. Wang, Y. Wang, Q. Huang, B. Cai, X. Qiu and Y. Tang, *J. Mater. Chem. A*, 2021, **9**, 11537-11544.

6 X. Wang, S. Yang, Y. Yu, M. Dou, Z. Zhang and F. Wang, *Cata.l Sci. Technol.*, 2020, **10**, 65-69.

7 C. Park, E. Lee, G. Lee and Y. Tak, *Appl. Catal. B-Environ.*, 2020, **268**, 118414.

8 E. A. Nagelli, F. J. Burpo, D. A. Marbach, A. N. Romero, D. J. Rabbia, H. W. Mahr, M. H. Jaskot, A. N. Murray and D. D. Chu, *J. Compos. Sci.*, 2020, **4**, 160.

9 Y.-C. Weng, C.-C. Wu, H.-J. Wang and Y.-Y. Wang, *Electrochim. Acta*, 2020, **340**, 136012.

10 D. Kaplan, M. Goor, L. Burstein, I. Popov, M. Shviro and E. Peled, *J. Solid State Electrochem.*, 2020, **24**, 2385-2393.

11 X. Tang, S. Zhang, J. Yu, C. Lu, Y. Chi, J. Sun, Y. Song, D. Yuan, Z. Ma and L. Zhang, *Acta*

Phys. Chim. Sin., 2020, **36**, 1906070.

12 B. Dembinska, A. Zlotorowicz, M. Modzelewska, K. Miecznikowski, I. A. Rutkowska, L. Stobinski, A. Malolepszy, M. Krzywiecki, J. Zak, E. Negro, V. Di Noto and P. J. Kulesza, *Catalysts*, 2020, **10**, 689.

13 M. Rethinasabapathy, S.-M. Kang, Y. Haldorai, N. Jonna, M. Jankiraman, G.-W. Lee, S.-C. Jang, B. Natesan, C. Roh and Y. S. Huh, *J. Ind. Eng. Chem.*, 2019, **69**, 285-294.

14 M. S. Garapati and R. Sundara, *Int. J. Hydrogen Energy*, 2019, **44**, 10951-10963.

15 R. Brandiele, V. Amendola, A. Guadagnini, G. A. Rizzi, D. Badocco, P. Pastore, A. A. Isse, C. Durante and A. Gennaro, *Electrochim. Acta*, 2019, **320**, 134563.

16 C. Zhang, Y. Dai, H. Chen, Y. Ma, B. Jing, Z. Cai, Y. Duan, B. Tang and J. Zou, *J. Mater. Chem*. A, 2018, **6**, 22636-22644.